Determination of subband structure, depolarization shift, and depletion charge in an $Al_xGa_{1-x}As$-GaAs heterostructure

K. Ensslin, D. Heitmann, and K. Ploog
Max-Planck-Institut für Festkörperforschung, Heisenbergstrasse 1, Postfach 80 06 65, D-7000 Stuttgart 80, Federal Republic of Germany
(Received 3 October 1988)

Resonant subband-Landau-level coupling (RSLC) spectroscopy is applied to study intersubband-resonance excitations in $Al_xGa_{1-x}As$-GaAs heterostructures. The carrier density N_s in our device can be tuned via a front gate voltage V_g in a controlled and reproducible way. The detailed analysis of the N_s dependence of the intersubband resonance and the comparison with a self-consistent calculation demonstrate that the anti-level-crossing in the RSLC experiment occurs at an energy $\tilde{E}_{10}$ which is shifted by the collective depolarization effect with respect to the subband separation E_{10}. From the same analysis we can also determine the depletion charge N_{depl} with an accuracy of 5%. This gives us the possibility to distinguish between a persistent photoeffect upon illumination arising first from carriers out of the GaAs buffer layer and later on from the doped $Al_xGa_{1-x}As$ region.

I. INTRODUCTION

Although modulation-doped $Al_xGa_{1-x}As$-GaAs heterostructures are widely used in application and fundamental research, the subband structure and the shape of the potential well are often only approximately known. The reason is that these quantities depend not only on the carrier density N_s, but also strongly on the depletion charge N_{depl}. The latter is often only estimated from the growth conditions and in addition depends in a sensitive manner on the cooling procedure and illumination of the sample. This makes it difficult to compare experiments[1–8] with self-consistent calculations.[9,10] If one is particularly interested in the dependence of the subband structure on the carrier density N_s in order to study self-consistent effects, Raman spectroscopy,[1,2] and luminescence[3] methods are limited since the presence of strong band-gap illumination causes quasiaccumulation conditions ($N_{\text{depl}} \approx 0$) and fixes N_s. Resonant–subband-Landau-level–coupling (RSLC) spectroscopy[4–6] has been applied using the illumination-induced persistent photoeffect[5,6] or a back-gate voltage[5] to vary N_s and N_{depl}. However, N_{depl} was only approximately known and, moreover, so far it was not clear from experiments whether the anti-level-crossing in the RSLC experiment occurs at the subband separation E_{10} ($E_{10}=E_1-E_0$, E_i is the energy of subband i) or at the depolarization-shifted intersubband resonance $\tilde{E}_{10}$. The latter case is expected according to the calculation of Zaluzny.[11] The importance of the depolarization shift on intersubband resonances in the two-dimensional electron gas (2D EG) in the Si metal-oxide-semiconductor (MOS) system was first pointed out by Chen *et al.*[12] Further calculations were performed for the Si system,[13] with inclusion of the exciton effect,[14] and for $Al_xGa_{1-x}As$-GaAs heterostructures.[9] In far-infrared (FIR) experiments the depolarization shift has so far been studied mainly for the Si-MOS system.[15–17] Recently also first results for the $Al_xGa_{1-x}As$-GaAs system from Raman[2] and FIR-stripline[8,18] experiments have been reported. Preliminary results of the depolarization effect in RSLC have been discussed in Ref. 7. Here we present an extended investigation of this phenomenon.

We have prepared modulation-doped $Al_xGa_{1-x}As$-GaAs heterostructures with large area semitransparent front gates, which allowed to change N_s in a controlled and reproducible way.[19,20] This gave us the possibility to study RSLC in detail in its dependence on N_s (see Fig. 1), while N_{depl} remained essentially unchanged. Comparison of the experimentally observed N_s dependence for the anti-level-crossing with a self-consistent calculation clearly reveals that the anti-level-crossing occurs at the depolarization-shifted energy $\tilde{E}_{10}$. In addition, using this comparison we can determine N_{depl}, which is the only adjustable parameter in our calculation, to an accuracy of 5%. This allows us to study the distinct behavior of the illumination-induced persistent photo effect.[21–23] We demonstrate that by a short illumination of the sample, at first electrons are excited from the depletion region, leading to an increase of N_s and a decrease of N_{depl}. Further illumination leads then to a further increase of N_s, whereas N_{depl} remains unchanged. We can thus determine whether photoexcited electrons originate from the GaAs buffer layer or from the Si-doped $Al_xGa_{1-x}As$ layer.

II. EXPERIMENT

The samples were grown by molecular-beam epitaxy and had the following configuration: 2.1-μm buffer layer and active GaAs, 18-nm $Al_xGa_{1-x}As$ spacer, 52-nm Si-doped $Al_xGa_{1-x}As$ ($x \approx 0.36$, $N_d \approx 5\times10^{17}$ cm^{-3}) and an 8-nm GaAs cap layer. The samples were mesa etched, defining gate areas of ≈ 3 mm diam. 100-nm Al_2O_3 (Ref. 24) followed by 5-nm NiCr were evaporated onto the gate area. Outside the gate area Ohmic contacts were an-

nealed to the 2D channel. Cyclotron resonance (CR) was measured in a 14.5-T superconducting magnet, which was connected via a wave-guide system to a Fourier transform spectrometer. Spectra were taken at fixed N_s and magnetic field B. The normal of the sample was slightly tilted ($\alpha \approx 5°$) with respect to the magnetic field to couple the motion of the electrons perpendicular and parallel to the 2D system.[4] The temperature was 2.2 K, and the resolution of the spectrometer was set to 0.1 cm^{-1}. A gate voltage V_g was applied between the gate and the channel contacts. The carrier density N_s was determined *in situ* under the conditions of the experiment from magnetocapacitance-voltage (MCV) measurements.[19] For illumination a red-light-emitting diode (LED) was mounted above the sample.

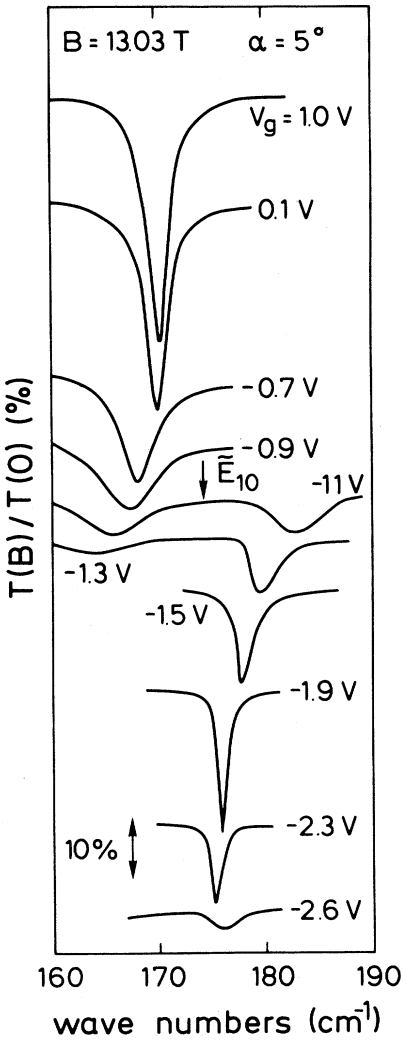

FIG. 1. Normalized transmission $T(B)/T(B=0)$ of unpolarized FIR radiation measured at fixed $B=13.03$ T for various gate voltages V_g. For $V_g \approx -1.1$ V the two resonances have approximately the same amplitude and linewidth and thus also the same oscillator strength. The arrow indicates the position of $\tilde{E}_{10}$.

In the following sections we want to give a very accurate comparison between theory and experiment. It is therefore necessary to explain in some detail the evaluation of our data. Figure 1 shows experimental spectra measured at fixed $B=13.03$ T for different V_g. Since V_g, N_s, and E_{10} are all monotonic functions of each other, we can tune V_g (and therefore E_{10}) so that the condition $E_{10} \approx \hbar\omega_c$ for the well-known RSLC occurs ($\omega_c = eB/m^*$, m^* is the cyclotron-resonance mass).[4] We have modeled the anticrossing behavior described in Sec. III by a simulation. We find that the energy level E_{ac}, determining the anticrossing, is given by $E_{ac} = \frac{1}{2}(E_h - E_l)$, exactly in the case when both resonances have the same oscillator strength. Here E_h and E_l denote the higher- and lower-frequency resonances, respectively. We will show later on that $E_{ac} = \tilde{E}_{10}$. The oscillator strengths in this case are defined by the projection of the wave functions $\Psi_0(\alpha)$ and $\Psi_1(\alpha)$ onto the unperturbed states $|0,1\rangle$ and $|1,0\rangle$ ($|n,m\rangle$ is the wave function of the nth subband and the mth Landau level for $\alpha=0$, see also Ref. 5). From the experimental spectra of Fig. 1 we can clearly see that for the anticrossing condition the two resonances have approximately not only the same amplitude but also the same linewidth. In addition, the amplitude

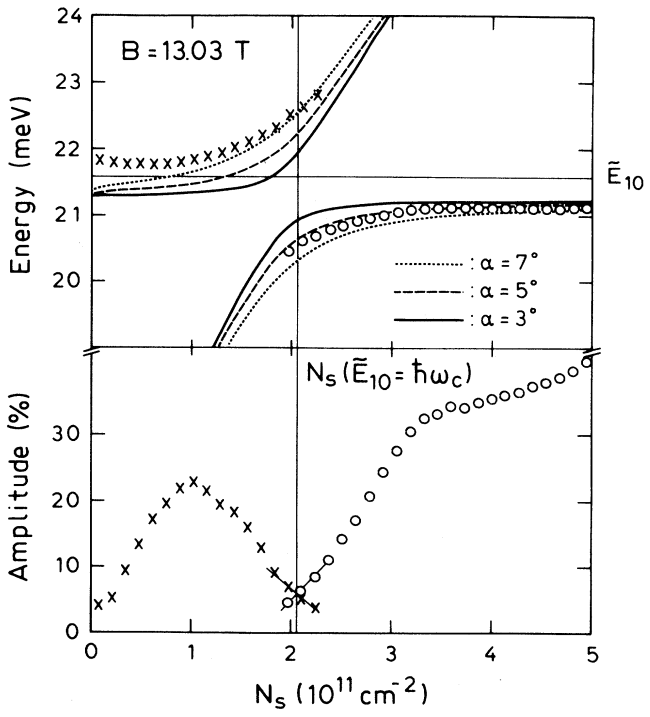

FIG. 2. Amplitude and resonance position from Fig. 1 plotted vs carrier density N_s. Circles (○) and crosses (×) mark lower and higher energy resonances, respectively. The straight lines show how the intersubband resonance $\tilde{E}_{10}$ and the corresponding N_s are obtained from the measurement. The curved lines in the upper part of the figure are the result of the coupling calculation for different tilt angles as indicated. The depletion charge was chosen to be $N_{depl} = 6.3 \times 10^{10}$ cm^{-3}.

and linewidth of both resonances develop symmetrically to the crossing condition. Thus, since the oscillator strength is a monotonic function of the amplitude (see Fig. 1), we can extract the values of $N_s(\tilde{E}_{10}=\hbar\omega_c)$ for the anticrossing in the lower part of Fig. 2 from the N_s position, where both resonances have the same amplitude. For different B, this procedure results in the experimental $\tilde{E}_{10}(N_s)$ curve. It is important to note that we can determine $\tilde{E}_{10}$ and the corresponding N_s from the experimental data to an accuracy of 1% and 5%, respectively.

III. CALCULATION OF COUPLING CONDITION AND DEPOLARIZATION EFFECT

In the case of a purely perpendicular magnetic field the Schrödinger equation can be completely separated in a term describing the motion of the carriers parallel to the interface (x,y) and perpendicular to the interface (z). Following Ando[25] we calculated the hybrid electric-magnetic subbands for a tilted magnetic field. In this case the Hamiltonian can be written as

$$H=H_\perp+H_\parallel+H' , \tag{1}$$

with

$$H_\perp=\frac{p_z^2}{2m^*}+V_{\text{eff}}(z)+\frac{\hbar^2}{2m^*}\frac{z^2}{l_\parallel^4} , \tag{2}$$

$$H_\parallel=\frac{p_x^2}{2m^*}+\frac{(p_y+eB_z x)^2}{2m^*} , \tag{3}$$

$$H'=\frac{\hbar}{m^*}\frac{zp_x}{l_\parallel^2} , \tag{4}$$

where $l_\parallel^2=\hbar/eB_y$. Here B_y and B_z are the components of the magnetic field parallel and perpendicular to the 2D EG, respectively. The potential $V_{\text{eff}}(z)$ is defined by the charge distribution and the conduction-band offsets.[9,10] Then one chooses as a basis

$$\Psi_{nNX}=\chi_N(x-X)\Theta_X(y)\phi_n(z)\exp\left[-i\frac{z_{nn}}{l_\parallel^2}(x-X)\right] \tag{5}$$

with χ_N, Θ_X, and ϕ_n being the usual eigenfunctions for $B_y=0$ corresponding to the quantum numbers N (Landau-level index), X (center coordinate), and n (subband index), respectively. We define

$$z_{nm}=\int_{-\infty}^{\infty}dz\,\phi_n(z)\phi_m(z)z . \tag{6}$$

The choice of this basis is convenient since the Hamiltonian then is diagonal with respect to the motion in the x-y plane if we can neglect coupling between different Landau levels of the same subband. Using $m^*/m_0=0.067$ we solved

$$H_\perp\phi_n(z)=E_n\phi_n(z) \tag{7}$$

self-consistently with numerically calculated wave functions. The boundary conditions are chosen according to a depletion approximation, which is described in more detail in the Appendix. The parametrization of the exchange correlation potential was the same as in Ref. 11. This gave us the matrix elements z_{nm}. To account for nonparabolicity effects we then chose $m^*/m_0=0.071$ (being the effective mass at $B=13$ T) and diagonalized H following Ref. 25. The lines depicted in Fig. 2 mark the result of this calculation for different values of α. Since $l_\parallel^2$ is a function of α, also $H_\perp$ depends on α. This means that the actual $E_{10}(N_s)$ curve is slightly ($\leq 2\%$) influenced by the parallel field component.

It is interesting to discuss the origin of the coupling with FIR radiation in the RSLC experiment. In FIR experiments without magnetic fields a component of the exciting electric field normal to the interface E_z is necessary to excite intersubband resonances. In experiments on Si-MOS systems special stripline,[15] prism,[16] or grating coupler[17] arrangements have been applied to create a suitable large-E_z component. For our experiments, with only a small tilt angle between the incident light and the sample normal, the z component of the electric field is negligibly small due to the high refractive index of the GaAs. This means that the intersubband resonance (ISR) is excited by the coupling to the CR rather than by the E_z component of the incident FIR radiation. We have hybrid electric-magnetic subbands in our system, but the observed resonance has still much more the character of a CR than of an ISR. As mentioned before, the small tilt angle leads to a coupling of the motion perpendicular and parallel to the 2D EG and the out of plane component of the Lorentz force accelerates the electrons in the z direction. This causes an effective charge-density excitation in z direction resulting in the depolarization shift of the optically observed intersubband resonance $\tilde{E}_{10}$ with respect to E_{10}. We considered depolarization and exciton effect following Ando[14] in the two-subband approximation by using the wave functions $\phi_n(z)$ from our self-consistent calculation. The resonance energy $\tilde{E}_{10}$ is related to the subband separation E_{10} by

$$\tilde{E}_{10}=E_{10}\sqrt{1+\alpha_{10}+\beta_{10}} \tag{8}$$

with

$$\alpha_{10}=2N_s\frac{e^2}{\epsilon_0\kappa}\frac{S_{11}}{E_{10}} , \tag{9}$$

$$\beta_{10}=-\frac{2N_s}{E_{10}}\int_{-\infty}^{\infty}dz\,\phi_1^2\phi_0^2\frac{\partial v_{\text{xc}}}{\partial n} , \tag{10}$$

$$S_{11}=\int_{-\infty}^{\infty}dz\left[\int_{-\infty}^{z}dz'\,\phi_1(z')\phi_0(z')\right]^2 . \tag{11}$$

Here v_{xc} is the exchange correlation potential, $n(z)$ the electron density distribution, and κ the dielectric constant of GaAs. The depolarization effect is described by α_{10}, the exciton effect by β_{10}. Figure 3 shows the results of our self-consistent calculation for $B=0$ of the subband separation E_{10} and the depolarization and exciton shifted intersubband resonance $\tilde{E}_{10}$ for different values of the depletion charge N_{depl} (see also Ref. 10). Varying N_{depl} shifts in particular all values of $\tilde{E}_{10}$ by a fixed amount leaving the slope of the $\tilde{E}_{10}$ versus N_s curve essentially unchanged.

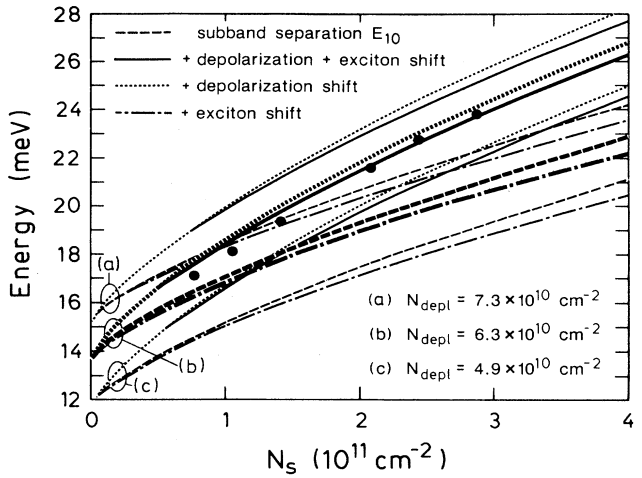

FIG. 3. Solid circles (●) mark experimental positions of the anticrossing. The lines are results of our self-consistent calculation of E_{10} and $\tilde{E}_{10}$, i.e., with and without exciton and depolarization effect, respectively. Different depletion charges are indicated. The thick solid line including exciton and depolarization effect for $N_{depl}=6.3\times10^{10}$ cm^{-2} describes the experimental data very well, indicating that the anticrossing occurs at the depolarization-shifted energy.

IV. RESULTS AND DISCUSSION

A. Subband structure

The only free parameter in our calculation is the depletion charge N_{depl} or the corresponding concentration of ionized acceptors N_A. The depletion charge N_{depl} is an important parameter in our evaluation. Its theoretical derivation will be explained in more detail in the appendix. Comparison with the experimental data in Fig. 3 shows that it is not possible to get agreement between experimental anticrossing energies and theoretical subband separation, E_{10} (e.g., without depolarization and exciton effects) by varying N_{depl}, because of the significantly different slopes of both quantities in their N_s dependences. However, an excellent agreement is found if both the depolarization effect and the exciton shift are included. This first shows that the anticrossing in the RSLC experiment occurs at the depolarization-shifted energy $\tilde{E}_{10}$ and second, knowing now that these effects are present and what their size is, it offers the possibility to determine N_{depl} and the corresponding N_A very accurately. In Fig. 3 we determine the value of $N_{depl}=6.3\times10^{10}$ cm^{-2}. So far, on samples without front gates,[5,6] $\hbar\omega_c$ was tuned to reach the crossing condition. In Figs. 2, 3, and 5 we chose a $\hbar\omega_c$ versus N_s plot to present the data. This plot manifests more clearly the existence of some additional effects on the CR beyond a simple one-particle effective-mass theory. Several investigations[20,26,27] have shown that m^* at least depends on nonparabolicity, filling factor, localization of the carriers, and interaction between transitions from different Landau and spin levels. Our presentation offers the possibility to extract the unperturbed RSLC.

For a further demonstration of the reliability of our theoretical understanding of the system we show in Fig. 4 anticrossing energies from a series of measurements at different magnetic fields. In this case the anticrossing occurs at different energies $\tilde{E}_{10}=\hbar\omega_c$ and different values on the N_s axis. The solid lines in Fig. 4 are the results of the coupling calculations mentioned above. To compare the results for different magnetic fields, the value of $m^*/m_0=0.071$ is used for all magnetic fields, although nonparabolicity is weaker at smaller magnetic fields. The

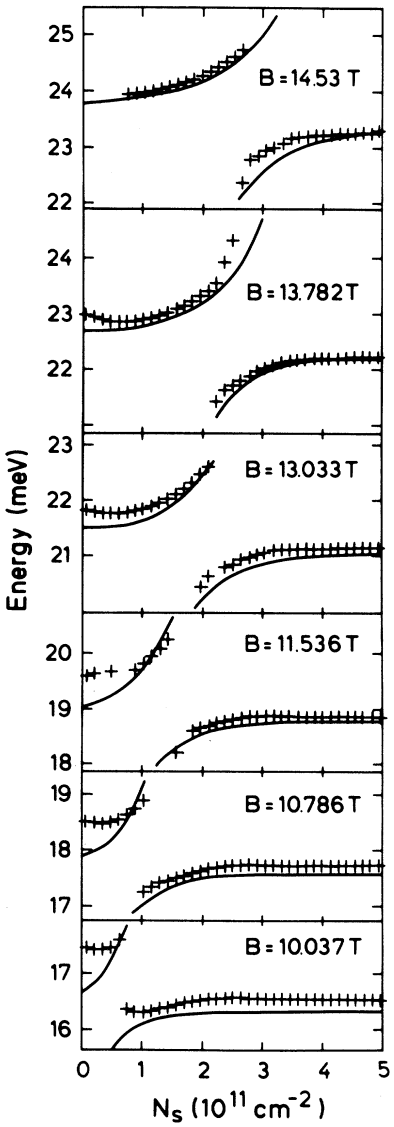

FIG. 4. Experimental resonance positions (+) vs carrier density for different magnetic fields. The solid lines are calculated resonance positions $\tilde{E}_{10}$ with $m^*/m_0=0.071$ to account for nonparabolicity near $B\approx13.5$ T. For these high magnetic fields the contribution of the confinement energy to the nonparabolicity is minor, since the system is in the quantum lines $\nu<2$. Concerning the calculation the depletion charge is $N_{depl}=6.3\times10^{10}$ cm^{-2}.

calculated energy splitting is proportional to the matrix element z_{10} and thus depends sensitively on the self-consistent potential and wave functions. For high magnetic fields there is satisfactory agreement reflecting the weak dependence of m^* on N_s.[20] This reveals that our theoretical modeling of the heterostructure is quite reliable. For lower magnetic fields it is much more difficult to evaluate the splitting for correspondingly small N_s accurately, since the oscillator strength and thus the signal-to-noise ratio is small, and the anticrossing decreases the amplitudes further (Fig. 1). Nevertheless we can clearly observe a deviation of the experimental points from the pure theoretical anticrossing behavior of $B=10.04$ T, which may be due to localization effects.

Figure 5 shows experimental resonance positions which have been measured after a different cooling cycle of the sample as compared to Fig. 3. Again the experimental values are best described by theory if all many-body effects are included in the calculation. For this cooling cycle we find $N_{\text{depl}}=5.7\times10^{10}$ cm^{-2} which is slightly different from Fig. 3. For high N_s and corresponding high values of B an additional shift is observed, presumably due to the diamagnetic shift at this high magnetic fields.

In our experiments we find that under typical conditions, i.e., $N_s=2.2\times10^{11}$ cm^{-2}, the depolarization shift is $\tilde{E}_{10}-E_{10}=2.6$ meV. From Raman spectroscopy[28] in heterostructures with $N_s=6.2\times10^{11}$ cm^{-2} a value of 3.8 meV was found, which is in excellent agreement with our results. In strip-line experiments[8] on $Al_xGa_{1-x}As$-GaAs heterostructures with the same carrier density as discussed here of $N_s=2.2\times10^{11}$ cm^{-2} a depolarization shift has been extracted which is more than about a factor of 2 smaller than our experimental results and the results from our calculation and from Ref. 15. It is not exactly known how large the influence of the highly conducting metal gate in the case of the strip-line experiment is.

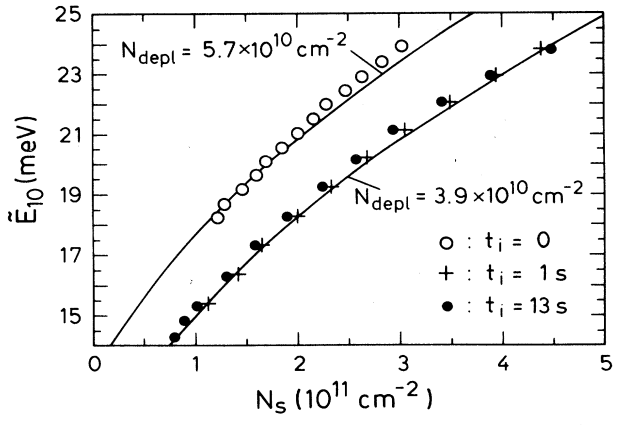

FIG. 5. Experimental intersubband-resonance energies vs carrier density for different illumination times t_i. The solid lines are results from our self-consistent calculation, including exciton and depolarization effect with the indicated values of N_{depl}. Note that the N_s values for the different N_{depl} values correspond to different V_g scales (see Fig. 7).

B. Effects of illumination upon depletion charge

The high accuracy to determine N_{depl} gives us the unique possibility to study in detail the effects of band-gap illumination on N_{depl}. The crosses (+) in Fig. 5 depict the experimental resonance positions that have been measured after a short illumination time $t_i=1$ s. The data for the illuminated sample are also excellently explained by the depolarization-shifted resonance $\tilde{E}_{10}$ for $N_{\text{depl}}=3.9\times10^{10}$ cm^{-2}. Further illumination ($t_i=13$ s) does not change N_{depl} any more; however, there is an increased number of carriers in the 2D EG at $V_g=0$. Figure 6 shows the carrier density at $V_g=0$, $N_{s0}=N_s(V_g=0)$, and $\Delta N_s=N_s(t_i)-N_s(t_i=0)$ as a function of illumination time t_i. In particular we find

$$N_{s0}(t_i=1\text{ s})-N_{s0}(t_i=0)=2.5\times10^{10}\text{ cm}^{-2}$$

and from the comparison with theory

$$N_{\text{depl}}(t_i=0)-N_{\text{depl}}(t_i=1\text{ s})=1.8\times10^{10}\text{ cm}^{-2}\ .$$

Recent investigations[21–23] have shown that there exist two main mechanisms for persistent photoconductivity in $Al_xGa_{1-x}As$-GaAs heterostructures. First, electrons can be photoexcited from the *DX* centers of the Si-doped $Al_xGa_{1-x}As$ and stay persistently in the 2D EG, because there is a high barrier for the reversed process. Second, the creation of electron-hole pairs in the GaAs leads to a charge separation due to the electric field in the depletion regions. The electrons are transferred to the 2D EG, some of the holes neutralize the ionized acceptors in the GaAs, and others move to the substrate. The latter process leads to a change in the slope of the potential and therefore changes the subband separation E_{10} at a certain fixed N_s. In the calculation the slope of the potential is completely described by the concentration of ionized acceptors and the usual depletion approximation (see the Appendix).

This reveals that in our experiment first nearly all the additional electrons in the 2D EG are transferred from the depletion charge, whereas further illumination excites electrons only from the highly doped $Al_xGa_{1-x}As$. This

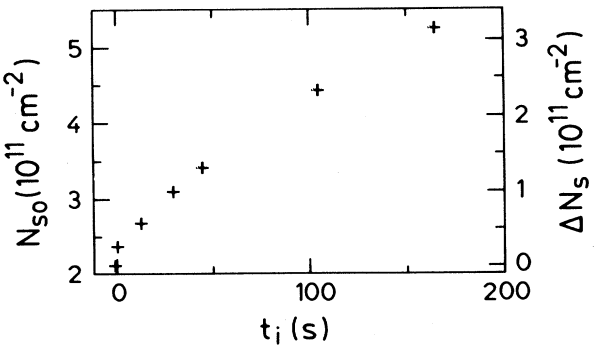

FIG. 6. Carrier concentration at zero-gate voltage $N_{s0}=N_s(V_g=0)$ vs illumination time. On the right-hand scale the density of additional carriers $\Delta N_s=N_s(t_i)-N_s(t_i=0)$ induced by illumination is indicated.

corresponds to the fact that the time constant for the excitation of the electrons from the *DX* centers is longer than for the creation and separation of electron-hole pairs in the GaAs. The amount of charge transfer from the GaAs buffer layer to the 2D EG is in agreement with a simple model,[22] which assumes that carriers from the GaAs buffer layer are induced as long as the conduction band becomes flat.

We next discuss some more details of the effect of illumination. In Fig. 7 we show MCV measurements for various values of t_i at $B=7.49$ T. For $t_i=1$ s the minima in MCV are more pronounced compared to the dark sample ($t_i=0$). This indicates an increase in dc mobility which is not only caused by the increase of N_s, but much more by the reduced number of ionized acceptors (see also Ref. 23). Further illumination ($t_i=13$ s, $t_i=45$ s) indicates that, due to the ionized donors, parallel conduction in the $Al_xGa_{1-x}As$ occurs, which smears out the MCV minima. It is possible to change N_s reproducibly with V_g for a wide range of t_i (see Fig. 6) up to $t_i=200$ s. For long illumination times $t_i>200$ s an increased concentration of ionized donors in the Si-doped $Al_xGa_{1-x}As$ is induced. Thus the maximum positive voltage V_g that can be applied without leakage currents decreases with increasing t_i. This is in agreement with theory, since leakage currents are expected to appear, when the Fermi energy is above the conduction band in the Si-doped $Al_xGa_{1-x}As$. Saturation illumination leads to considerable leakage currents for all $V_g\neq 0$ and then it is not possible to change N_s via V_g any more.

Finally we note another interesting finding. From the experiment we can conclude that it is not possible to achieve $N_{\text{depl}}=0$ in a persistent mode, i.e., without constant illumination. Strictly speaking the depletion approximation does not hold anymore for $N_{\text{depl}}=0$. However, for the experimentally observed value of $N_{\text{depl}}=3.9\times10^{10}$ cm^{-2} the depletion approximation should still be valid. We can thus estimate the finite-depletion charge by the following simple model. The dissociation field of the excitons in GaAs can be estimated by the binding energy (≈ 5.4 meV) and the corresponding Bohr radius ($r\approx 10$ nm) to be about 5 kV/cm. This means that we need a finite slope of the potential in the GaAs buffer layer to separate the electron-hole pairs. If we assume a parabolic electrostatic potential $\Phi(z)$ with boundary conditions

$$\Phi(z=0)=0\ , \tag{12}$$

$$\Phi(z=d_{\text{depl}})=-E_g/e\ , \tag{13}$$

$$\frac{d\Phi}{dz}(z=d_{\text{depl}})=0\ , \tag{14}$$

and the Poisson equation

$$\epsilon_0\kappa\,\Delta\Phi=eN_A\ ,$$

the maximum electric field $E=d\Phi/dz$ is

$$E(z=0)=\left[\frac{2N_AE_g}{\epsilon_0\kappa}\right]^{1/2}.$$

Here $z=0$ marks the position of the 2D EG and d_{depl} the length of the depletion region. Taking $E(z=0)=5$ kV/cm we estimate a minimum value of $N_A=5\times10^{13}$ cm^{-3} corresponding to $N_{\text{depl}}=3.2\times10^{10}$ cm^{-2}. This result is consistent with the experiment.

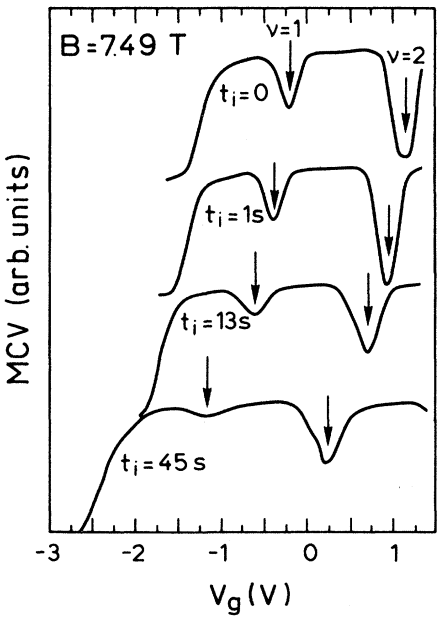

FIG. 7. Experimental MCV curves for fixed $B=7.49$ T and various illumination times. Arrows indicate positions of filling factors $\nu=1$ and $\nu=2$ ($\nu=N_sh/eB$).

V. CONCLUSIONS

We have demonstrated experimentally that the anticrossing in a RSLC experiment occurs at the intersubband resonance energy $\tilde{E}_{10}$, which is shifted with respect to the subband separation E_{10} by the depolarization effect. The comparison between experiment and theory allowed us to determine N_{depl} very accurately and to study N_{depl} in its dependence on illumination. We can thus determine that upon first illumination electrons are photoexcited only from the GaAs buffer layer. Further illumination then excites electrons from the highly doped $Al_xGa_{1-x}As$ layer. The excellent agreement between theory and experiment reveals the good theoretical understanding of wave functions and subband energies of $Al_xGa_{1-x}As$-GaAs heterostructures.

ACKNOWLEDGMENTS

We would like to thank K.v. Klitzing for valuable discussion and acknowledge financial support of the Bundesministerium für Forschung und Technologie, West Germany.

APPENDIX: DESCRIPTION OF DEPLETION APPROXIMATION

We have seen in the evaluation of our experimental data that N_{depl} is a very important parameter which we

can determine with a high accuracy. We provide here the theoretical description, how we considered the depletion charge in our calculation, in particular, how it depends on N_A and the corresponding d_{depl}.

We define the following geometry: $z=0$ is the position of the $Al_xGa_{1-x}As$-GaAs interface where the 2D EG is situated, s is the thickness of the $Al_xGa_{1-x}As$ spacer, l is the thickness of the Si-doped $Al_xGa_{1-x}As$ layer, and t the thickness of the GaAs cap layer. The spatial distribution of fixed charges in the heterostructure can then be written as

$$\rho(z)=\begin{cases}0, & -t-l-s\le z\le -s-l\\ eN_d, & -l-s\le z\le -s\\ 0, & -s\le z\le 0\\ -eN_A, & 0\le z\le d_{\text{depl}}\ ,\end{cases} \tag{A1}$$

where the depletion length d_{depl} can be calculated from the other sample parameters. The concentrations of ionized donors and acceptors are described by N_D and N_A, respectively. The distribution of the free carriers is given by

$$f(z)=\sum_i N_i\phi_i^2(z) \tag{A2}$$

with

$$N_i=\frac{m^*kT}{\pi\hbar^2}\ln\left[1+\exp\left[\frac{E_F-E_i}{kT}\right]\right]\ . \tag{A3}$$

The length $A>0$ is defined such that the wave functions have fully decayed to 0,

$$\int_{-\infty}^{A} f(z)=N_s\ . \tag{A4}$$

In addition we define

$$F_A=\int_{-\infty}^{A}\cdot dz\int_{-\infty}^{z}\cdot d\bar{z}\,f(\bar{z}) \tag{A5}$$

and

$$u=s+l+t\ , \tag{A6}$$

which will be needed later on. The Poisson equation reads

$$\epsilon_0\kappa\frac{d^2\Phi}{dz^2}(z)=ef(z)-\rho(z)\ . \tag{A7}$$

There are three boundary conditions for the electrostatic potential $\Phi(z)$.

(1) $\Phi(z)$ is fixed on the surface of the sample by the Schottky-barrier height E_s, the gate voltage V_g, and the Fermi energy E_F:

$$\Phi(z=-u)=-\frac{1}{e}(E_s-E_F)+V_g\ . \tag{A8}$$

(2) For $z>d_{\text{depl}}$ the potential Φ is flat:

$$\frac{d\Phi}{dz}(z>d_{\text{depl}})=0\ . \tag{A9}$$

(3) In addition, assuming unintentionally p-doped material, for $z>d_{\text{depl}}$ the Fermi level lies in the valence band:

$$\Phi(z=d_{\text{depl}})=-\frac{1}{e}(E_{\text{gap}}-E_F)\ . \tag{A10}$$

Two integration constants from the Poisson equation and the depletion length d_{depl} are determined by these three boundary conditions. The integration of the Poisson equation leads then to the analytic exact expression:

$$d_{\text{depl}}=-u+\left[u^2+\frac{F_A-N_s(A+u)+N_D(l^2/2+lt)+\frac{\epsilon_0\kappa}{e^2}(E_{\text{gap}}-E_s+eV_g)}{N_A/2}\right]^{1/2}\ . \tag{A11}$$

The threshold voltage V_{th} corresponds to $V_g(N_s=0)$. A simple capacitance formula yields

$$eN_su=\kappa\epsilon_0(V_g-V_{\text{th}}) \tag{A12}$$

such that V_g can be eliminated from Eq. (25). The term F_A-N_sA partially cancels and is 2 to 3 orders of magnitude smaller than the rest. This means that d_{depl} is essentially independent of N_s, as is expected from the experiment. Such $u\ll d_{\text{depl}}$ we can now write in a very good approximation:

$$d_{\text{depl}}\approx\left[\frac{N_D(l^2/2+lt)+\frac{\epsilon_0\kappa}{e^2}(E_{\text{gap}}-E_s+eV_{\text{th}})}{N_A/2}\right]^{1/2}\ . \tag{A13}$$

In the self-consistent calculation we fixed N_D, such that V_{th} equals the experimental threshold voltage. The obtained values for N_D ($N_D\approx3\times10^{17}$ cm^{-3}) agree very well with those estimated from the growth conditions. The depletion charge N_{depl} is then given by

$$N_{\text{depl}}=N_Ad_{\text{depl}}=\sqrt{2N_A}\left[N_D(l^2/2+lt)+\frac{\epsilon_0\kappa}{e^2}(E_{\text{gap}}-E_s+eV_{\text{th}})\right]^{1/2}\ . \tag{A14}$$

For one particular sample this depletion approximation is valid in a strict sense only for an infinitely slow cooling cycle and no illumination, i.e., for thermal equilibrium conditions. As we have discussed in Sec. IV B two processes influence N_{depl}: (a) neutralization of ionized acceptors, i.e., a change in N_A, and (b) transfer of holes to the substrate, i.e., a decrease of d_{depl} and the formation of quasi-Fermi levels. Under real conditions, i.e., no thermal equilibrium, both processes are present on illumination and cooling. We did not consider the formation of quasi-Fermi levels, since this has no significant influence on our results of N_{depl} and would give an additional free parameter. In our calculations we assume [see the boundary conditions (A8)–(A10)] neutralization of acceptors to be the dominant process. Within this description we find the following values of N_A and d_{depl}:

N_{depl} (10^{10} cm^{-2})	N_A (10^{14} cm^{-3})	d_{depl} (10^{-4} cm)
3.9	0.7	5.6
4.9	1.1	4.4
5.7	1.5	3.8
6.3	1.8	3.5
7.3	2.5	2.9

[1]G. Abstreiter and K. Ploog, Phys. Rev. Lett. **42**, 1308 (1979).
[2]A. Pinczuk, J. M. Worlock, H. L. Störmer, R. Dingle, W. Wiegmann, and A. C. Gossard, Solid State Commun. **36**, 43 (1980).
[3]I. Kukushkin, V. Timofeev, K. v. Klitzing, and K. Ploog, *Festkörperprobleme,* edited by U. Rössler [Adv. Solid State Phys. **28**, 21 (1988)] (Vieweg, Braunschweig, 1988).
[4]Z. Schlesinger, J. C. M. Hwang, and S. J. Allen, Phys. Rev. Lett. **50**, 2098 (1983).
[5]G. L. J. A. Rikken, H. Sigg, C. J. G. M. Langerak, H. W. Myron, J. A. A. J. Perenboom, and G. Weimann, Phys. Rev. B **34**, 5590 (1986).
[6]A. D. Wieck, J. C. Maan, U. Merkt, J. P. Kotthaus, K. Ploog, and G. Weimann, Phys. Rev. B **35**, 4145 (1987).
[7]K. Ensslin, D. Heitmann, and K. Ploog, in *Proceedings of the Conference on High Magnetic Fields in Semiconductor Physics,* edited by G. Landwehr (Springer, Würzberg, 1988).
[8]A. D. Wieck, K. Bollweg, U. Merkt, G. Weimann, and W. Schlapp (unpublished).
[9]T. Ando, J. Phys. Soc. Jpn. **51**, 3893 (1982).
[10]F. Stern and S. Das Sarma, Phys. Rev. B **30**, 840 (1984).
[11]M. Zaluzny, Solid State Commun. **56**, 235 (1985).
[12]W. P. Chen, Y. J. Chen, and E. Burstein, Surf. Sci. **58**, 263 (1976).
[13]S. J. Allen, Jr., D. C. Tsui, and B. Vinter, Solid State Commun. **20**, 425 (1976).
[14]T. Ando, Z. Phys. B **26**, 263 (1977).
[15]P. Kneschaurek, A. Kamgar, and J. F. Koch, Phys. Rev. B **14**, 1610 (1976).
[16]B. D. McCombe, R. T. Holm, and D. E. Schafer, Solid State Commun. **32**, 603 (1979).
[17]D. Heitmann and U. Mackens, Phys. Rev. B **33**, 8269 (1986).
[18]A. Seilmeier, H. J. Hübner, G. Abstreiter, G. Weimann, and W. Schlapp, Phys. Rev. Lett. **59**, 1345 (1987).
[19]K. Ensslin, D. Heitmann, H. Sigg, and K. Ploog, Surf. Sci. **196**, 263 (1988).
[20]K. Ensslin, D. Heitmann, and K. Ploog, Phys. Rev. B **37**, 10 150 (1988).
[21]A. Katalsky and J. C. M. Hwang, Solid State Commun. **51**, 317 (1984).
[22]E. F. Schubert, A. Fischer, and K. Ploog, Solid State Electron. **29**, 173 (1986).
[23]J. J. Harris, D. E. Lacklison, C. T. Foxon, F. M. Selten, A. M. Suckling, R. J. Nicholas, and K. W. J. Barnham, Semicond. Sci. Technol. **2**, 783 (1987).
[24]Al_2O_3 suppresses leakage currents, an idea of J. Richter (private communication).
[25]T. Ando, Phys. Rev. B **19**, 2106 (1979).
[26]F. Thiele, U. Merkt, J. P. Kotthaus, G. Lommer, F. Malcher, U. Rössler, and G. Weimann, Solid State Commun. **62**, 841 (1987).
[27]E. Batke, H. L. Störmer, A. C. Gossard, and J. H. English, Phys. Rev. B **37**, 3093 (1988).
[28]A. Pinczuk and J. M. Worlock, Surf. Sci. **113**, 69 (1982).